ElectroPhotonic Analysis (EPA) of tap water droplets versus hydro-alcoholic solutions

Marc Henry(✠)[1], Pierre Dorfman[2], Michel Van Wassenhoven[3*], Martine Goyens[4]
[1] University of Strasbourg, France
[2] M.R.C. Endowment Fund, Private Academy of Science™, Meyzieu, France.
[3] Coordinator of DynHom Research Project, Chastre, Belgium.
[4] Pharmaceutical Association for Homeopathy, Wepion, Belgium

*Corresponding author, michel@forest128.be, Rue Taille Madame 23, B-1450 Chastre, Belgium.

Received: Jun 28, 2025 **Revised**: Sep 30, 2025 **Just Accepted Online**: Oct 14, 2025
Published: Xxx

Please cite this article as:
M. Henry, P. Dorfman, M. Van Wassenhoven, M. Goyens (2025) ElectroPhotonic Analysis (EPA) of tap water droplets versus hydro-alcoholic solutions. **Substantia**. *Just Accepted*. DOI: 10.36253/Substantia-3597

Abstract
Aim: The lack of precision of validated electrochemical identification methods and the limited detection of compounds at low concentrations by spectrometric methods are well known. Physics has provided a strong theoretical background, and modern technologies allow the development of electro photonic analytical devices that aim to provide greater precision in the detection of compounds, even at low concentrations. This original article provides a new experimental and theoretical insight into chemistry.
Method: This paper describes the theory and the technical aspects of the electro photonic analysis method. This technology is tested on samples of tap water droplets compared to hydro-alcoholic solutions (ethanol 62% m/m).
Results: Using repeated measurements on the same tap water and ethanolic solutions, we demonstrate the reproducibility of the method. This method can now be systematically double-blind tested on a variety of samples.

Keywords
Electrophotonic analysis, Corona discharge, Validation, Reproducibility, Discriminatory potential, Photon electrochemistry.

Introduction

Water is a complex substance characterized by thermodynamic coefficients displaying a highly non-linear change with temperature or pressure [1]. One of the most amazing properties of liquid water is its ability to reduce its volume upon heating between 0°C and 4°C. Galileo already discussed such an anomaly about four hundred years ago [2]. Water is also an essential element for life and for many religious beliefs [3]. Among all known substances, water displays the highest ratio of Boyle's temperature to molecular weight [4]. Moreover, considering cosmic abundances of the elements in the universe one gets the following order: hydrogen > helium > oxygen [5]. Consequently, as helium is an unreactive gas, water is also the most abundant substance of the universe. To best realize the strangeness of water, one may rely on the fact that upon heating, molecules should acquire more kinetic energy, allowing them to increase the volume holding them together. This is not the case with liquid water where more thermal energy below 4°C leads to a reduction in volume. It is not an easy matter for science to explain such an amazing fact. In fact, only quantum physics deal easily with such a phenomenon [6, 7]. Basically, the anomaly comes from the formation of coherence domains that also explains why water, a diamagnetic substance, is strongly affected by magnetic fields [8]. This has the amazing consequence of being able to synthesize a DNA-molecule from scratch using electromagnetic information [9,10]. Hydrogen bonding plays a key role in corona discharges in water by influencing cohesion and the stability of hydrated electrons, which are formed and react via hydrogen bonds during the process [11,12]. Another sequel is that water is expected to play a crucial role in the manifestation of consciousness in living beings [13]. The fact that liquid water may acquire a nanostructure (coherence domains) by coupling with the fluctuating electromagnetic fields filling the quantum vacuum helps understanding, for instance, how high dilutions may have a biological effect despite the absence of any solute species [14,15].

However, as coherence concerns quantum phases that are not physically observable, conventional physico-chemical measurements are of very limited use. There is a need to use non-conventional techniques, for characterization of the information stored in these putative coherence domains. Among such techniques, we may cite electrochemical impedance spectroscopy (EIS) [16], aqua-photomics [17], evaporated water droplets patterns [18] or sensitive crystallization [19]. Alternatively, one may use lyophilization techniques to recover solid residues analyzed by more conventional techniques [20]. Herein, we have applied a technique, named electrophotonic analysis (EPA) based on Corona discharges [21-24]. This technique is well adapted for studying solids or liquids. It has proven to be very sensitive, producing images that can be quantitatively analyzed using classical procedures in medical imaging.

2. Background

Corona discharges also known as St. Elmo's fires are well-documented natural phenomena that were already known in ancient Greece. About sixty years ago, a corona-based technique named "Kirlian photography" was developed in Russia [25]. The idea was to record a photographic image of an object after applying a large electric potential between the object and a dielectrically isolated electrode. As such a technique, called corona discharge photography (CDP) may be applied to human subjects, it has rapidly been claimed that variations in image structure can be related to changes in

physiological, psychological and psychic states [26]. Further studies have revealed that upon application of a high voltage (15-60 kV) to matter, a few electrons are first produced between the object and the isolated electrode. Further acceleration of these electrons by the electrical field provokes ionization of the surrounding gas (generally air). This leads to an exponential growth in the number of electrons and positive counter-ions. The electrons sweep quickly toward the positive anode, while the cluster of positive ions moves somewhat more slowly toward the negative cathode. When the positive ion cluster in the air gap reached a critical density, many recombination events with electrons occur. Such events lead to a large emission of light photons in the UV-region of the electromagnetic spectrum having also a tail in the visible region (bright blue color). The cluster of positive ions then becomes brightly illuminated with both positive and negative streamers between the electrodes. Consequently, discrete balls of light move in various directions.

Rigorous experiments have shown that charge recombination processes create streamer images extending radially from the sample- electrode boundary [27]. It was observed that for a given voltage pulse and pulse repetition rate, the streamer range is dependent on the electric field bending due to the mismatch of dielectric constants et dielectric interfaces, the relative thickness of the dielectric components between the sample and the voltage source, the water vapor content of the atmosphere and the geometric characteristics of sample's surface.

More particularly, this range is proportional to the corona onset voltage. It is an inverse function of the resistance formed by the high-voltage anode and the sample. For a given resistance, water vapor reduces streamer range by absorbing photons which otherwise would be available for propagating positive streamers by photoionization. Water vapor may also reduce streamer breakdown voltage by influencing the charge sheath that forms above a positive point.

The absence of streamers within a given region of the sample-electrode boundary is predominantly due to the release of water present on or within the sample.
The existence of corona streamers that deviate significantly from a radial trajectory is another phenomenon that is related to moisture. Accordingly, streamers that have curved paths usually outline regions in which streamers are absent, and frequently curve into these empty regions, electrons being attracted there by a positive density of charges sustained by water molecules.

Consequently, streamer curvature is not observed when the samples are dry. It follows that most of the variations in the images of corona of a sample in contact with the anode may be accounted for by the presence of moisture on or within the sample's surface. During exposure, moisture is transferred from the sample to the anode and causes an alteration of the electric charge pattern on the anode, hence the electric field at the surface of the sample. As a result, large variations in the density of corona images as well as corona streamer range and trajectories may be brought about.

For biological substances, it has been confirmed that light emission mirrors the moisture content and geometry of the object [28]. In the case of living tissues, no evidence was related to the activity of either plant or animal cells. No evidence of any property of the corona pattern could be related to the physiological, psychological or psychic condition of the samples [29]. It was also concluded that CDP could contribute to those areas in science where conductivity and surface arrangement of the conducting areas play a major role [30]. More recent studies have however concluded that there was mounting evidence that CDP diagnosis for living tissues has an important part to

play within both orthodox and complementary therapies in medicine [31]. More research is thus needed on this technique that could lead to very complex images.

It was also shown that photographic material was not necessary for recording halo, streamers and other details typical of CDP photographs [32]. Such images may then be recorded on any bulk dielectrics and on thin films of various materials deposited on glass substrates. A significant advance in this field was the possibility of using modern optics; electronics and computer processing leading to the so-called gas discharge electro photon capture (EPC) analysis based on gas discharge visualization (GDV) technique [33]. It has then been claimed that EPC can be implemented as an express method for assessment of treatment procedures effectiveness, evaluating emotional and physical conditions of people [33]. The technique seems to be sensitive enough to detect temperature, air humidity, air pressure, gender, age, heartbeat, and blood pressure effects on recorded images after a short contact with various textiles [34]. Another interesting aspect of the technique is the possibility of detecting weak transformation of water under the influence of electromagnetic fields, air, light and other subtle factors [35]. Finally, the EPC/GDV technique has also previously been used for investigating the concentration dependence of corona discharges around drops of inorganic electrolytes [36].

The motivation of this study was then to check if electrophonic analysis (EPA) could be a valuable scientific tool for differentiating among various kinds of liquid water samples, mixed or not with alcohol. The spirit was to use a highly sophisticated device developed by the company CORAMP solutions based in Brens (France) and to use a large set of image analysis techniques for retrieving information embedded in EPA images. As any piece of matter contains a variable amount of water, it follows that corona discharge imaging may be very useful in the detection and quantification of moisture or others compounds in animate or inanimate specimens through the orderly modulation of the image due to various levels of these compounds. It was further hoped that differences observed in corona images might also reflect a change in liquid as well as interfacial water.

3. Methods

3.1 Experimental setup

Our measuring device (figure 1) is based on a Advanced Electro Photonic Generator (AEPG©). It is able producing a stable and reproducible electromagnetic field both in voltage and frequency. This generator, coupled with other components controlled by highly reliable electronics, produces with its strong pulse voltage, an electromagnetic field on the electrode plate. This field is alternately positive and negative, with a predefined frequency. This field successively mobilizes electric charges at the surface and in the thickness of the object to be analyzed causing ionization of the gaseous environment around the studied body (plasma gas). This ionization creates an electronic avalanche, which by splitting the gas molecules, release UV photons that are recorded by the Hamamatsu camera. All these phenomena don't appear simultaneously, but one after the other, depending on the pulse generator. Images acquisition provides an idea of the statistical distribution of light emission during exposure time. Numerous experiments have shown that charges are mainly distributed in two different ways:

− The positive pulses of the generator, leading to filamentary structures called "streamers".

− The negative pulses creating rounded and globular forms called "coronae".

These acquisitions enable an appreciation of the increasing richness of the image as the complexity of the analyzed object grows.

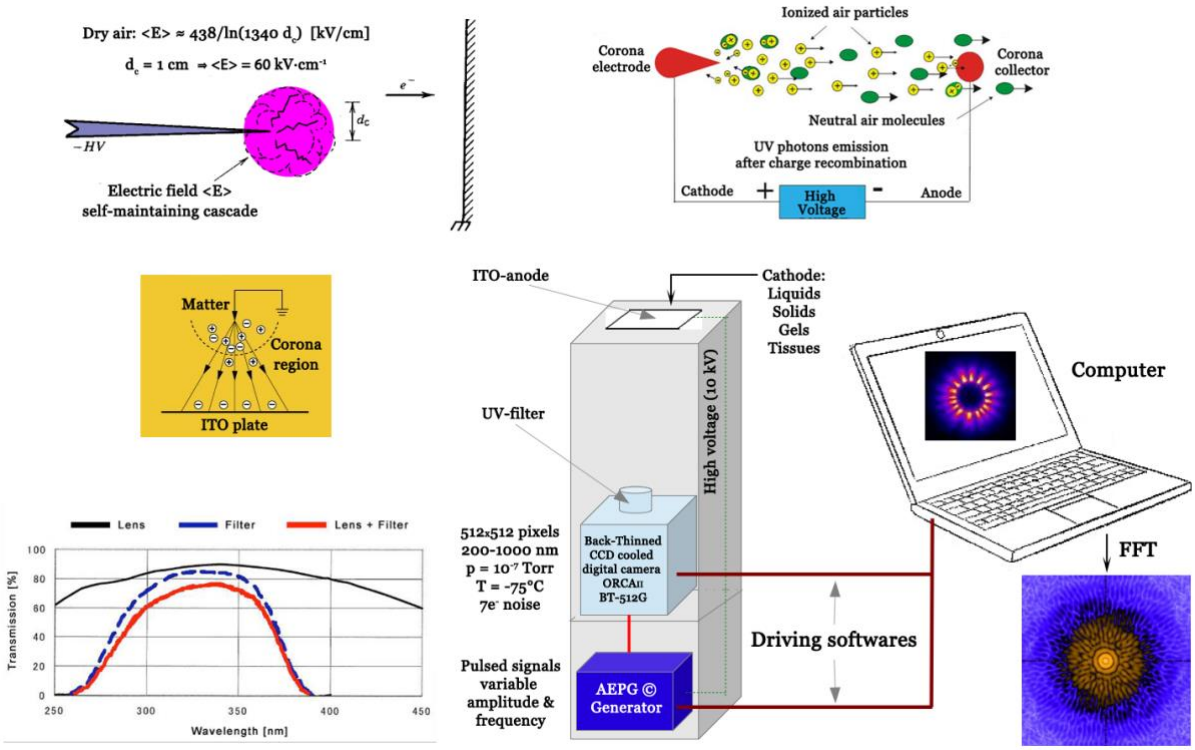

Figure 1: *Principles of the corona effect and experimental device for recording electrophotonic images.*

To this generator is attached an EFUSE© a transparent and conductive electrode plate having the highest possible homogeneity at each point of its surface allowing good control of the distribution of electrical charges. For recording the photonic emission, we have used a Hamamatsu HD camera (ORCA IIBT 512G2) with a specific timing and adjustable exposure time coupled to an optical equipped with a UV filter.

It is worth noticing that many environmental physical factors are to be taken into account in conducting electrophotonic experiments. Among them, we may cite: ambient atmosphere (gas), moisture (crucial factor for ionization), and dust (highly sensitive to electric fields). Table 1 gives the recorded experimental conditions concerning acquisition of the images.

Table 1: *Conditions in the laboratory during acquisition of electrophotonic images.*

Parameter	Value
T(inside) /°C	19
T(outside) /°C	20
R.H. %	78
Voltage / kV	11
Frequency / Hz	110
Weather	sunny

Figure 2 shows the experimental setup used for recording images on water droplets.

A total of 12 images have been captured of Brens' tap water droplets. The measures were implemented in September 2019. The aim was to establish whether it was possible to obtain reproducible images of identical droplets using a technique that is renowned for being highly sensitive to environmental factors. Minerals in used tap water are: Calcium: 88.7 mg/L; Potassium: 0.9 mg/L; Magnesium: 9.8 mg/L; Sodium: 3.2 mg/L; Sulphates: 8.9 mg/L.

Other measurements were carried out as part of a test of the technique in March 2016 (comparable experimental parameters). Three images of a concentrated mother tincture of Gelsemium were compared to three images of the same ethanol/water percentages without plant extract (appropriate control). The aim was to establish whether this method could distinguish between these preparations. These measurements were taken in a double-blind manner, meaning that the researcher did not know which sample was being analyzed.

Another 12 images correspond to strongly diluted (above the Avogadro number) plant extract (Gelsemium) in a mix of ethanol/deionized water (62% m/m of ethanol) were finally compared to the tap water results. The aim was to extend the comparison between tap water and the alcohol/water mixture.

These measures are preliminary and are intended solely to verify the method's validity and its potential for further development. The characterisation of other liquid water samples (mineral water, seawater, contaminated water, water subjected to vortex or electromagnetic fields, homeopathic remedies, etc.) could be reported in future papers. Different percentages alcohol/water mix could also be measured. The choice of 62% m/m ethanol concentration is necessary as an appropriate control for Gelsemium mother tincture.

Figure 2: *Experimental setting for recording electrophotonic images on water or liquid droplets.*

The volume of the analyzed droplet is maximized as closely as possible to the moment it falls from the pipette. Ideally, for a new prototype, a computer would determine this volume, and an automated pipette would perform pipetting to avoid possible small volume variations.

Other experimental parameters in 2016: Millipore RX 45 series water apparatus, serial number FSDM 96292D; Ethanol 96%V/V Ph.Eur. in 1-liter bottles Certa. Batch

15H20-C01-16756 P.23 09 2015 Exp. 08 2018. Verg.nr.597R01872 UN1170; 500 ml bottle of Gelsemium Sempervirens HAB Heel mother tincture, supplied by Homeoden in a PET bottle. Batch 548463. Expiry date: 12/2018/ 982 UH 911F34

To extend the measurements to other types of solution, we plan to use AI. This will require us to multiply the number of measurements several hundredfold in order to generate a database of reference images.

Several strategies are available for computer analysis of EPA images, free of subjective estimation. The first strategy is to determine the center of the investigated object followed by the determination of its border. Then, one could study the angular dependence of luminosity with a fixed resolution of a few degrees. From angular dependence, the streamers that are more or less prominent radial ray-like formations, are determined and their characteristics (height, width, etc.) calculated. Using this technique, it was possible to evidence distinct behavior of corona discharges patterns as regards ionic composition of salts in water, both radially and angularly [37]. If such a method seems well adapted for drops of solutions, it cannot be used for solids where streamers are systematically very short and very thin and hardly discernable from a more or less globular halo. New strategies have thus been developed for automatic analysis of EPA images. The strategy is a detailed analysis of the shapes that may be recognized in the pictures and analyzed in terms of geometric parameters. A second strategy is to perform the same kind of tasks on a spatial Fourier transform of the images.

3.2 Image processing 3.3 Contrast enhancement 3.4 Color enhancement 3.5 Thresholding algorithms 3.6 Geometrical analysis (See Supplementary material)

3.7 *Measured parameters*

The measurements are repeated on different well-defined areas of the colored and FFT images obtained. 2 areas for the colored versions, 5 areas for the FFT views. Figure 3 is an example of the development of one of these images. Figure 4 allows us to compare 3 source images of pure ethanol 62% m/m and of the mother tincture of a plant Gelsemium sempervirens containing also ethanol 62% m/m.

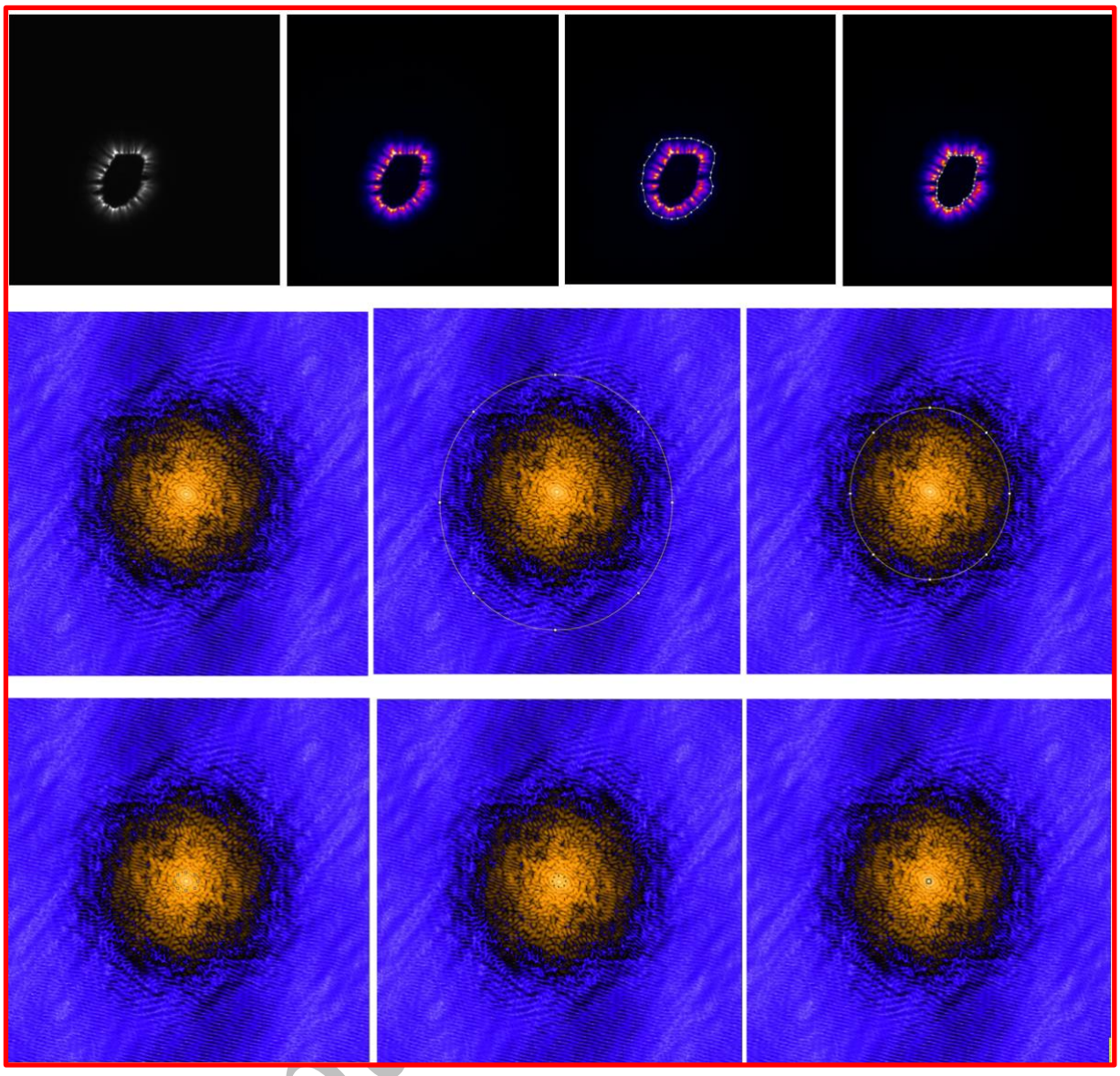

Figure 3: *Black and white, colored and FFT image and the selected surfaces on a water droplet (external selection, brightest selection, center 1, 2 and 3).*

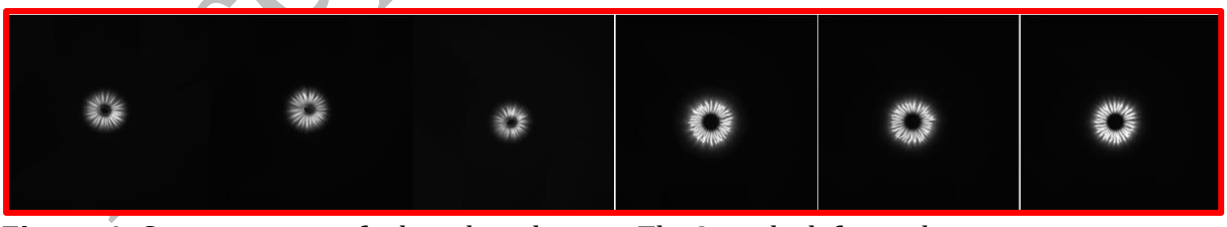

Figure 4: *Source images of ethanolic solutions. The 3 on the left are the pure hydroalcoholic solution, on the right the 3 images of the mother tincture of the plant Gelsemium. Both solutions contain 62% m/m of ethanol.*

3.8 *Normalization of data*

Data normalization aims to transform the values of the dataset into the same scale [92-94]. For multiple data sets where variability is justified by measurements that can be influenced by technical or environmental factors, standardization on one parameter is appropriate. For EPA, the internal areas analyzed must be comparable in size.

3.9 *Statistical analysis*
All statistical analyses were performed on EPA raw data using SigmaStat version 4, a wizard-based statistical software package designed to guide users through each step of the procedure. For multiple comparisons, two- or three-way analyses of variance (ANOVAs) were applied after the normality (Shapiro–Wilk test) and equality of variances (Brown–Forsythe test) were validated. The following specific pairwise multiple comparison procedures were suggested: The Tukey test for two-way ANOVA and the Holm-Sidak method for three-way ANOVA. The significance level was set at 0.05.

4. Results

One of the main advantages of recording EPA images is the extreme sensitivity of the technique. It may then be anticipated that small changes around the droplet, atmosphere's temperature as well as relative humidity or electromagnetic background could lead to completely different images for the same sample. To check further this point, twelve images have been captured for tap water.

As a preliminary step, six images were analyzed using the Weber algorithm and five local adaptive thresholding techniques (Bernsen, Niblack, Sauvola, Phansalkar, and Savakis). Reproducibility at the 95% level was observed for all these parameters (Table 2) between these six images.

Table 2: *Results of statistical analysis using five local adaptive thresholding techniques. for parameters of the 6 first tap water photographs.*

Statistics (6-values) for the sample: tap water with prob = 95.0%.							
Indice	Mean	σ	EIQ	Low	High	Asymm.	Flat.
L2-N	1514382	415201	103834	1078655	1950108	-0.7521	-1.2426
H1-N	771101	341254	195312	412977	1129225	-0.2303	-1.6639
0-D	8522	1648	332	6793	10252	-1.0410	-0.5675
½-D	1201	293	113	894	1509	-0.9368	-0.7445
1-D	213	44	17	167	259	-0.9140	-0.8301
2-D	110	17	6	92	127	-0.9541	-0.7872
∞-D	62	6	2	55	68	-0.8679	-0.9402
1-H	7.7051	0.3441	0.1056	7.3440	8.0663	-1.0590	-0.6001
2-λ	0.0093	0.0017	0.0008	0.0075	0.0112	1.1328	-0.4852
1-E	0.5911	0.0121	0.0049	0.5784	0.6038	-0.9175	-0.8714
2-E	0.9044	0.0085	0.0023	0.8955	0.9133	-1.0915	-0.5574

The analysis described in section 3.7 has been applied to a second set of 12 analyzed images to check reproducibility once more.

A/ In terms of the global image (without area selection), the area geometry parameters are always the same. Table 3 shows the coefficients of variability for the other parameters of 12 tap water source photographs. Table 4 shows these variances for the 7 selected areas (2 colored and 5 FFT images see Fig 3).

Table 3: *Coefficients of variability looking at the images without any area selection (global image) for parameters of the 12 tap water photographs.*

Measured parameters	Global Black & White	Global coloured	Global FFT
Mean	2%	7%	13%
StdDev	6%	4%	3%
Mode	0%	4%	26%
Min	0,7%	0%	0%
Max	0%	2%	1%
XM	0,6%	2%	0%
YM	1%	3%	0%
Median	0,3%	3%	16%
Skew	6%	6%	62%
Kurt	12%	17%	>100%

Table 4: *Coefficients of variability between parameters of the 12 tap source photographs calculated for the selected areas.*

Measured parameters	Color External selection	Color Internal selection	FFT External selection	FFT Brightest Selection	FFT Center 3	FFT Center 2	FFT Center 1
Area	6%	8%	19%	16%	26%	12%	32%
Mean	8%	5%	3%	2%	2%	1%	1%
StdDev	8%	3%	3%	3%	10%	11%	12%
Mode	7%	4%	3%	2%	2%	4%	3%
Min	3%	2%	4%	22%	10%	6%	5%
Max	0%	3%	0%	0%	0%	0%	0%
X	2%	2%	1%	1%	0,1%	0,2%	0,1%
Y	3%	3%	2%	0 ,7%	0,2%	0,1%	0,2%
XM	3%	2%	1%	0 ,9%	0,1%	0,2%	0,1%
YM	3%	3%	1%	0,6%	0,1%	0,1%	0,2%
Perim	3%	6%	9%	8%	12%	5%	15%
BX	3%	3%	21%	7%	0,9%	0,2%	0,3%
BY	5%	5%	22%	9%	0,8%	0,2%	0,3%
Width	3%	6%	10%	8%	13%	6%	16%
Height	5%	9%	10%	10%	12%	8%	16%
Major	5%	8%	9%	9%	13%	5%	17%
Minor	4%	6%	9%	8%	12%	8%	16%
Angle	3%	28%	73%	88%	0%	>100%	>100%
Circ	3%	6%	2%	5%	0,9%	0,4%	1%
Feret	5%	8%	9%	9%	13%	0,5%	17%
Median	14%	3%	3%	3%	0,1%	0,1%	2%
Skew	12%	15%	24%	35%	99%	64%	>100%
Kurt	23%	36%	66%	57%	57%	77%	61%
FeretX	10%	4%	46%	32%	0,9%	0,1%	0,4%
FeretY	24%	17%	24%	20%	0,2%	0,1%	0,4%
FeretAngle	40%	34%	73%	88%	0%	>100%	>100%
Min Feret	3%	8%	9%	8%	12%	8%	14%
AR	6%	12%	4%	6%	0,8%	7%	11%
Round	6%	12%	4%	5%	0,7%	6%	10%
Solidity	1%	3%	0%	0%	0,9%	2%	8%

B/ To test the potential of the method to discriminate between two images, we compared first, 3 images of pure ethanolic solution and 3 of a concentrated mother tincture. Both are titrated to 62% m/m ethanol (figure 4).

Analyzing these 6 images, only 2 of the 30 parameters related to the vertical axis of the image (Y, YM) did not pass the 3-way ANOVA test. This statistical approach allows us to check the ability to discriminate between two different products, but also between the selected areas. It also provides another way of checking the reproducibility of the method. Normality test passed everywhere except for Mode and FeretX. Variance passed everywhere. Discrimination between ethanol and mother tincture (product) was successful for 20 parameters for the outer perimeter selection and for 18 parameters for the central dark area. Failures are expected because, in these hydroalcoholic images the shape is perfectly round, in which case the angular parameters cannot be used for differentiation.

Table 5: *Statistical analysis of the indexes measured on the electrophotonic images. Highlighted in pink are results statistically significant (p=<0.05) in favor of discrimination.*

Measured parameters	Ethanol		Gelsemium		ANOVA-3w	Normality	Variance	P-value between		
	Mean	StdDev	Mean	StdDev				Product (n=2)	Zone (n=2)	Sample (n=3)
Area	4875	4152	11173	10784	OK	Passed	Passed	0,034	<0.001	0,845
Mean	81824	17709	51227	38175	OK	Passed	Passed	0,006	<0,001	0,919
StdDev	46983	9037	45339	34092	OK	Passed	Passed	0,862	0,004	0,958
Mode	26	17	132	135	OK	Failed	Passed	0,037	0,013	0,991
Min	8	1	6	1	OK	Passed	Passed	<0.001	1,000	<0.001
Max	224	38	177	86	OK	Passed	Passed	0,046	<0.001	0,784
X	247	3	241	1	OK	Passed	Passed	<0.001	0,190	0,238
Y	272	2	273	1	NS	Passed	Passed	0,264	0,787	0,583
XM	247	3	240	1	OK	Passed	Passed	<0.001	0,877	0,355
YM	271	2	273	1	NS	Passed	Passed	0,094	0,578	0,738
Perim.	224	116	324	206	OK	Passed	Passed	0,019	<0.001	0,869
BX	211	20	189	34	OK	Passed	Passed	0,005	<0.001	0,733
BY	237	19	222	32	OK	Passed	Passed	0,022	<0.001	0,791
Width	72	36	104	66	OK	Passed	Passed	0,023	<0.001	0,897
Height	71	37	103	65	OK	Passed	Passed	0,016	<0.001	0,836
Major	72	37	104	66	OK	Passed	Passed	0,020	<0.001	0,899
Minor	70	37	102	65	OK	Passed	Passed	0,018	<0.001	0,836
Angle	15	37	45	49	NS	Passed	Passed	0,334	1,000	0,772
Circ.	0,998	0,003	1,000	0,000	NS	Passed	Passed	0,130	0,203	0,358
Feret	72	37	104	66	OK	Passed	Passed	0,020	<0.001	0,897
Median	74	15	34	28	OK	Passed	Passed	<0.001	<0.001	0,779
Skew	0,584	0,122	1,623	0,656	OK	Passed	Passed	0,006	0,096	0,993
Kurt	-0,361	0,199	2,397	2,760	OK	Failed	Passed	0,027	0,045	0,993
FeretX	219	20	209	42	NS	Passed	Passed	0,578	0,107	0,703
FeretY	281	22	293	30	NS	Passed	Passed	0,481	0,406	0,722
FeretAngle	15	37	45	49	NS	Passed	Passed	0,334	1,000	0,772
MinFeret	70	37	102	65	OK	Passed	Passed	0,018	<0.001	0,837
AR	1,036	0,038	1,028	0,024	OK	Passed	Passed	0,531	0,031	0,093
Round	0,967	0,034	0,974	0,022	OK	Passed	Passed	0,553	0,027	0,096
Solidity	0,996	0,002	1,003	0,006	OK	Passed	Passed	0,038	0,563	0,711

About the reproducibility of the measurements between the 3 samples of the same product, the difference in the mean values between them is not so great as to exclude the possibility that the little differences are simply due to random sampling variability (Table 5 - Figure 5).

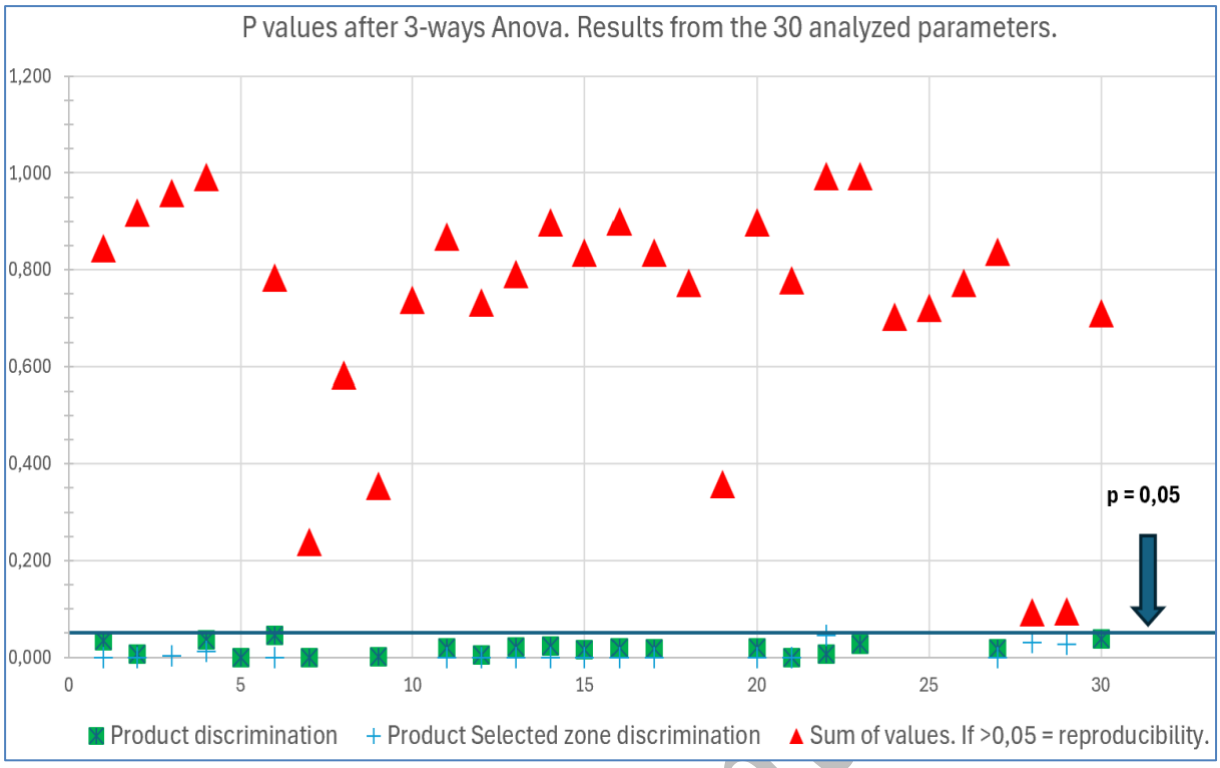

Figure 5: *Statistical analysis of the parameters measured on the electrophotonic images.*

The same analysis can be done on the selected areas of the FFT images (Fig 3). However, we can see that the outermost central zone 3, which is clearly visible in the Gelsemium mother tincture image, is missing from the ethanol FFT images (Fig 6). The 3 ethanol images have only 2 concentric circles, hexagonal in the middle, whereas the images of the tinctures of Gelsemium, like the tap water drops above, have a third additional circle around the center. This discrimination is possible because a specific luminous wavelength is expressed for Gelsemium, but not for ethanol. For the remaining 4 selected shared areas the 3-way ANOVA procedure has been followed for the 30 parameters, aiming to assess the potential for discrimination between these two products. Analyses of the other areas did not enable them to distinguish between the wavelengths of light emitted by ethanol control and the Gelsemium mother tincture.

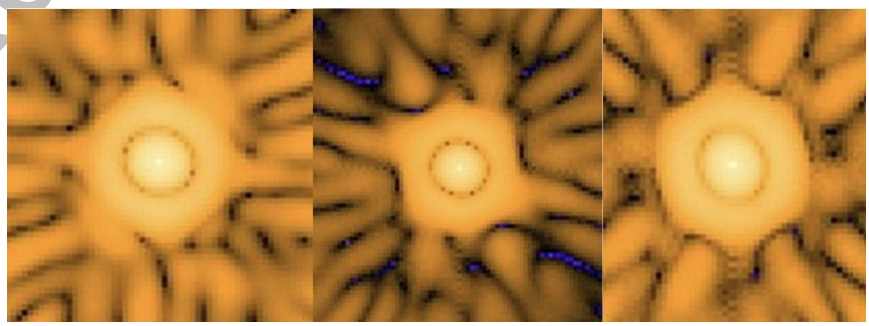

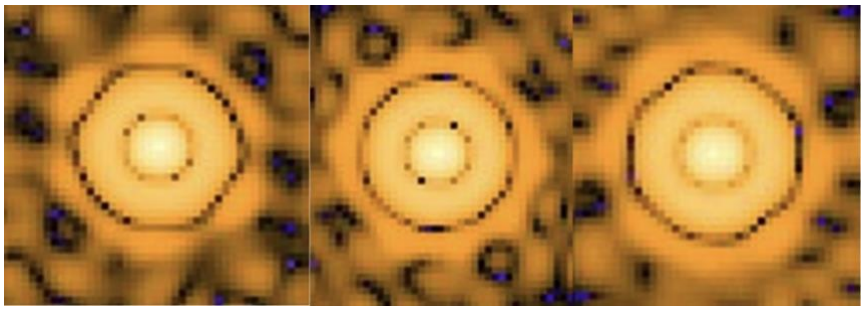

Figure 6*: The central areas of the three images of 62% ethanol are shown above. The three images of the Gelsemium mother tincture, which also has a 62% alcohol content, are shown below.*

C/ The third stage of this validation is to compare the above mentioned 12 images of drops of tap water with 12 images of Gelsemium (62%m/m), at very high dilutions. The solvent used for these dilutions is an alcohol/water mixture titrated to 62% m/m ethanol. These images were taken randomly over 4 consecutive days (Figure 7). Small natural variations in temperature and humidity at the sites must be considered.

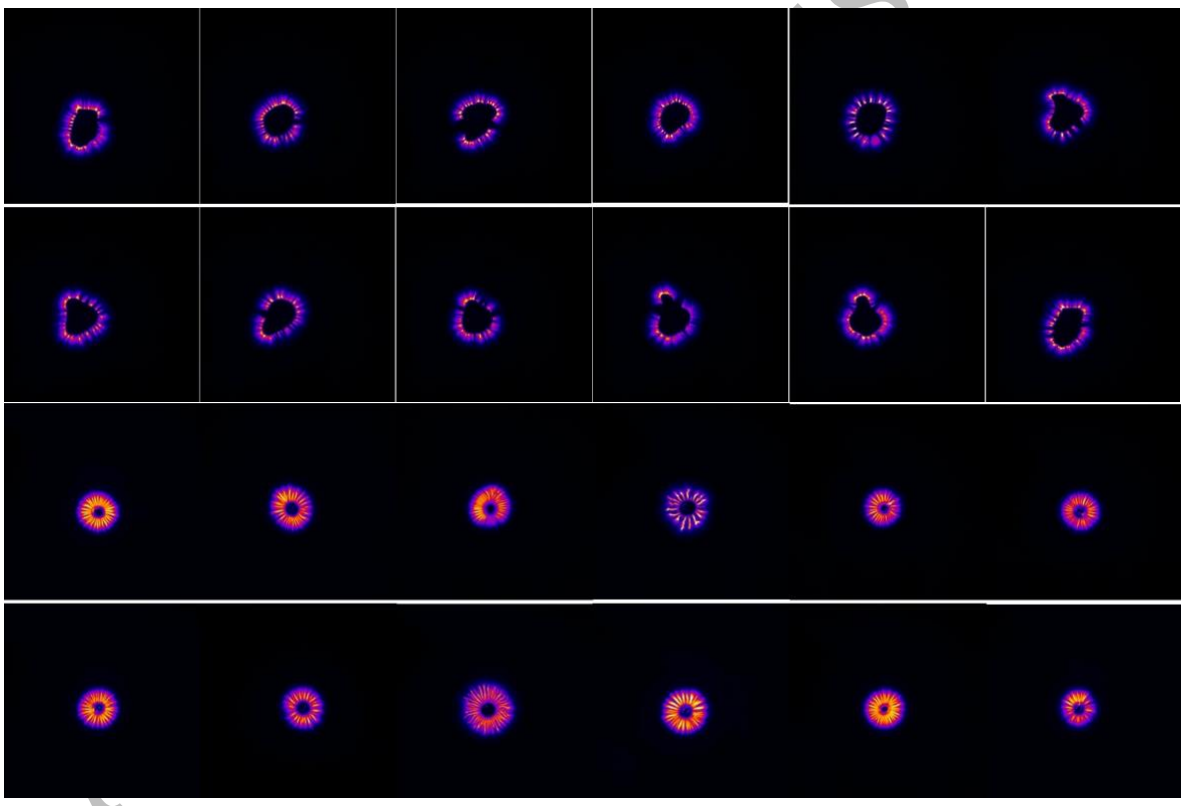

Figure 7: *12 images of drops of tap water above and below 12 images of high diluted Gelsemium.*

The differences between tap water and hydroalcoholic solutions of Gelsemium are obvious (Fig 7). Streams are longer for Gelsemium, dark center is larger for tap water images.

For the global images of tap water considering all measured parameters the mean CV is 1% and for Gelsemium 4%.

As the images are circular in shape, the angle values (or related parameters) are irrelevant when it comes to the selected external or internal area of Gelsemium, just like they are for tap water.

Considering the other parameters, during the area selection process, the variability of measurements is greater for Gelsemium than for tap water. The other parameters will also be affected by the instability of the size of Gelsemium images. The coefficient of variation for all parameters in the two selected zones (external and internal) is around 38%. Therefore, the size of the internal area needs to be normalized before the other parameters can be analyzed (Table 6).

Table 6: *The coefficient of variation for tap water is spontaneously acceptable. To obtain comparable values for Gelsemium images, the perimeter of the selected internal area, corresponding to the perimeter of the observed drop, must be normalized before analyzing all other parameters.*

		Normalized
	TAP WATER	Gels 10^{-26} 10^{-48}
INTERNAL AREA	Perim	Perim
1	293.521	109.978
2	300.628	119.401
3	255.899	111.532
4	277.329	130.419
5	287.148	125.664
6	291.420	108.391
7	260.011	105.249
8	244.352	116.239
9	297.342	124.098
10	255.256	113.119
11	278.361	108.391
12	288.899	106.814
Mean	277514	114941
SD ET	18995	8232
CV	0,0684	0,0716
CV%	7%	7%

Using a 2-way ANOVA (product/samples) for the external area, the normality and variance tests were passed for almost all parameters. Discrimination between products is statistically significant. For 26 parameters even at $p<0.001$. Among the 12 samples of each product, no significant difference can be observed.
For the internal area, results are the same, discrimination between products is statistically significant everywhere, for 27 parameters even at $p<0,001$.

D/ FFT images are focused on light wavelength of emitted light and do not need to go through a normalization process (Figure 8). The center corresponds to a large spatial wavelength. Wavelengths become shorter and shorter towards the periphery.

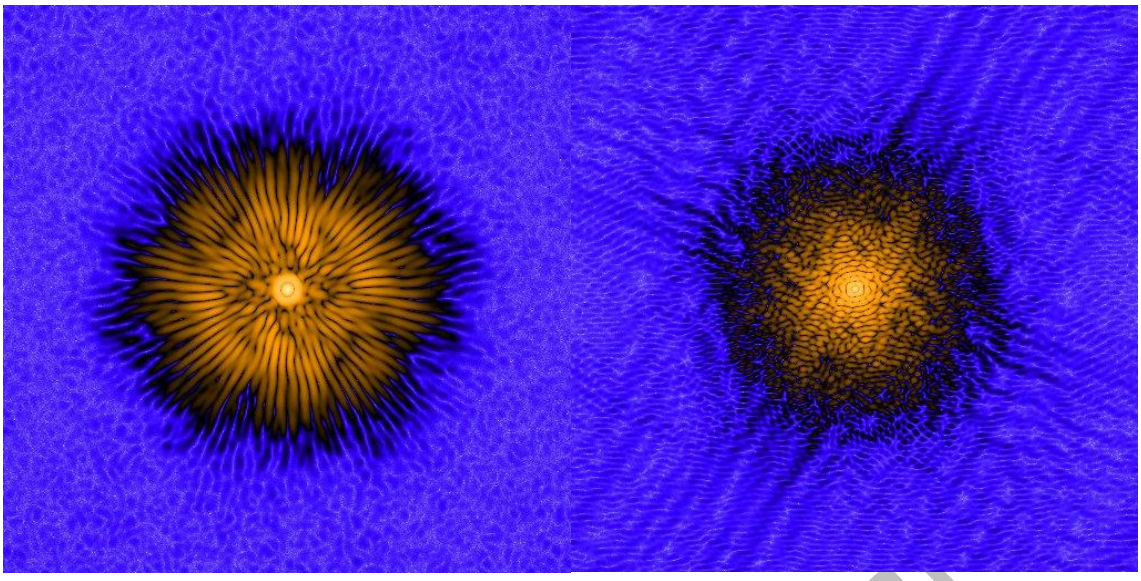

Figure 8: *On the left is an FFT image of a highly diluted Gelsemium drop. On the right is an FFT image of a drop of tap water, for example.*

The first observed result is that all the FFT images of Gelsemium dilutions have only 2 central concentric zones (Fig 8) before streamers are expanding outside, just like pure ethanol (Fig 6). On the contrary, the FFT images of the tap water are more complex in the center; the streamers have a different structure.

The differences in the wavelengths of the emitted light are obvious even without statistical analysis. Using 3-way ANOVA, the parameters related to the selection of the area are specific and the difference is highly statistically significant ($p<0,001$) for product and zone, but there is no statistically significant difference between the different samples of the same product (Perim; BX; BY; Width; Hight; Major; Minor; Feret; MinFeret). The same result is obtained for the intensity of the emitted light expressed in pixels (StdDev; Min). Kurtosis is also discriminant.

Detailed ANOVA spreadsheets in **supplementary material**.

5. Conclusion

The electro-photonic analytical approach is a valuable tool for gaining theoretical insights into chemistry. There are several reasons why these insights can be validated in practice. This validation needs to be confirmed using more data.

- The photographs of different samples of the same composition show reproducible results with a reliable coefficient of variation, which is a significant advantage of the method.
- The approach can detect measurable differences in the concentration of two comparable high-ethanolic solutions (with or without added material), which is important for achieving experimental accuracy.
- Even when the internal area, corresponding to a different volume of the drop has to be normalized, the method can distinguish between common tap water and highly diluted plant extract (Gelsemium).

6. Acknowledgment

We would like to thank Professor Marc Henry's children (CARA) for granting us permission to publish this article posthumously. We would also like to thank CARA & Biodynamizer for providing the missing photographs that enabled us to finalize this article. Our thanks also go to Mr Vieilledent and Heeren, who built the EPA prototype used for these measurements. Finally, we would like to thank the DynHom team for their help in finalizing this article.

7. Conflict of interest

No conflict of interest.

References

[1] Emiliano Brini, Christopher J. Fennell, Marivi Fernandez-Serra, Barbara Hribar-Lee, Miha Luksĭc, Ken A. Dill, "How Water's Properties Are Encoded in Its Molecular Structure and Energies", Chem. Rev., 2017, 117, 12385-12414.
[2] P. Lo Nostro & B. W. Ninham, « Aqua Incognita: Why Ice Floats on Water and Galileo 400 Years on », Connor Court Pub., Ballarat (2014).
[3] Marc Henry, « The state of water in living systems: from the liquid to the jellyfish ». Cell Mol. Biol. (2005), 51: 677-702.
[4] Marc Henry, "Water and its mysteries". Inference : Int Rev. Sci., 4, n°3, March 2019 https://inference-review.com/article/water-and-its-mysteries.
[5] Marc Henry, "Water and the periodic table", Susbtantia (2019), 3(2) Suppl. 3: 9-11. doi: 10.13128/Substantia-701.
[6] I. Bono, E. Del Giudice, L. Gamberale, M. Henry, « Emergence of the Coherent Structure of Liquid Water », *Water* (2012), **4**, 510-532.
[7] S. Sen, K. S. Gupta, J. M. D. Coey. « Mesoscopic structure formation in condensed matter due to vacuum fluctuations ». *Phys. Rev. B* (2015), **92** :155115.
[8] Marc Henry, « The topological and quantum structure of zoemorphic water », in Aqua Incognita: Why Ice Floats on Water and Galileo 400 Years on, P. Lo Nostro & B. W. Ninham Eds, Connor Court Pub., Ballarat (2014), chap IX, 197-239.
[9] L. Montagnier; J. Aïssa; A. Capolupo; T. J. A. Craddock; P. Kurian; C. Lavallée; A. Polcari; P. Romano; A. Tedeschi; G. Vitiello, « Water bridging dynamics of polymerase chain reaction in the gauge theory paradigm of quantum fields », *Water (MDPI)* (2017), **9** : 339-357
[10] B. Qing Tang; Tongju Li; Xuemei Bai; Minyi Zhao; Bing Wang; Glen Rein; Yongdong Yang; Peng Gao; Xiaohuan Zhang; Yanpeng Zhao; Qian Feng; Zhongzhen Cai; Yu Chen, « Rate limiting factors for DNA transduction induced by weak electromagnetic field », *Electromagnetic Biology and Medicine* (2019), 38(1) : 55-65.
[11] Ignatov, I.; Marinov, Y.G.; Vassileva, P.; Gluhchev, G.; Pesotskaya, L.A.; Jordanov, I.P.; Iliev, M.T. Nonlinear Hydrogen Bond Network in Small Water Clusters: Combining NMR, DFT, FT-IR, and EIS Research. *Symmetry* 2025, *17*, 1062.
[12] Tomaz Urbic, Ions increase strength of hydrogen bond in water, Chemical Physics Letters, Volumes 610–611, 2014, Pages 159-162,
[13] M. Henry, « Consciousness, Information, Electromagnetism and Water », *Substantia* (2020), 4(1): 23-36.
[14] Marc Henry, « Fisica y quimica de las altas diluciones », *Rev. Med. Homeopat.* (2017), 10(2) : 41-52.

[15] M. Henry, “The physics and chemistry of high dilutions”, VIIth National Congress of Homeopathy, San Sebastian, Spain, May, 6-8, (2016). Reprinted in “Homeopathy and You” (2019), Vol. 5, n°2 March, n°3 April.
[16] C. Soares, J.A. Tenreio Machado, Antonio M. Lopes, E. Vieira, C. Delerue-Matos, “Electrochemical impedance spectroscopy characterization of beverages”, Food Chemistry, (2020), 302: 125345.
[17] E. B. van de Kraats, J. S. Muncan, R. N. Tsenkova (2019), “Aqua-photomics - Origin, concept, applications and future perspectives”, Substantia 3(2) Suppl. 3: 13-28. doi: 10.13128/ Substantia-702.
[18] Maria Olga Kokornaczyk, Sandra Würtenberger, Stephan Baumgartner, (2020) « Impact of succussion on pharmaceutical preparations analyzed by means of patterns from evaporated droplets », *Sci Rep.,* **10**, 570. https://doi.org/10.1038/s41598-019-57009-2.
[19] C. Cimpean, C. Hotiu, “Sensitive crystallization – a valuable method for analyzing informational quality of food supplements” (2014), *Bull. Transilvania University of Brasov*, Series II, 7(56) : 85-92.
[20] Vittorio Elia, Elena Napoli, Roberto Germano, Valentina Roviello, Rosario Oliva, Marcella Niccoli, Angela Amoresano, Maria Toscanesi, Marco Trifuoggi, Antonio Fabozzi, Tamar A. Yinnon, "Water perturbed by cellophane: comparison of its physicochemical properties with those of water perturbed with cotton wool or Nafon", J. Thermal Analysis Calorimetry (2020), https://doi.org/10.1007/s10973-020-10185-0.
[21] G. Vieilledent, R. Herren, M. Henry, V. Morard, Quynh Nhu Xuan Trinh Kramer, « New applications of Corona discharges for photonics characterization of inert or living matter », http://www.electrophotonique.com/news/, BioEM2014, Cape Town, South Africa, Jun 08 - 13, 2014.
[22] Y. Creyghton, E. Veldhuizen & W.R. Rutgers. Electrical and Optical Study of pulsed Positive Corona. In Non-Thermal Plasma Techniques for Pollution Control. 205-230, 1993.
[23] Goldman, M. & Goldman, A. & Sigmond, R.. The corona discharge, its properties and specific uses. Pure and Applied Chemistry 57. 1353-1362, 1985.
[24] Leonard Loeb. Electrical coronas: their basic physical mechanisms. University of California Press Berkeley and Los Angeles 1965 ISBN 978-0520007659.
[25] Kirlian, S.D. Kirlian W. C. (Fotografirovanie i wizualnoje nabludenie pri posredstwie took wysokiej czastoty. Jurnal naucznoj i prok3adnoj fotografii i kinematografii), « The photography and visualisation of matter by the means of high frequency current », *Russ. J. Sci. Appl. Photogr. Cinematogr.* (1961), 6 : 397-403.
[26] William A. Tiler, « Are psychoenergetic pictures possible ? », *New Scientist* (1974), 25 April, 160-163.
[27] J. O. Pehek, H. J. Kyler, D. L. Faust, « Image Modulation in Corona Discharge Photography », *Science* (1976), 194 : 263-270.
[28] Andrew A. Marino, Robert O. Becker, Betsy Ullrich, Jon Hurd, « Kirlian photography: potential use in diagnosis », *Psychoenergetics systems* (1979), 3 : 47-54.
[29] Arleen J. Watkins, William S.Bickel. « A study of the Kirlian effect », *Skeptical Inquirer* (1986), 10(3): 244-257, Spring.
[30] Arleen J. Watkins, William S.Bickel. « The Kirlian technique: controlling the wild cards», *Skeptical Inquirer* (1989), 13(2): 172-184, Winter.
[31] J. G. Gadsby, « Kirlian photography diagnosis – a recent study », *Complementary Therapies in Medicine* (1993), 1 : 179-184.

[32] John Opalinski, « Kirlian-type images and the transport of thin-film materials in high-voltage corona discharges », *J. Appl. Phys.* (1979), 50(1) : 498-504.
[33] K. G. Korotkov, P. Matravers, D. V. Orlov, B. O. W. Williams, « Application of electro photon capture (EPC) analysis based on gas discharge visualization (GDV) technique in medicine : a systematic review », *J. Alternative and Complementary Med.* (2010), 16(1) : 13-25.
[34] Izabela L. Cieseilska, « Images of corona discharges as a source of information about the influence of textiles on humans », AUTEX Research J. (2009), 9(1) : 36-41.
[35] K. Korotkov, D. Orlov, « Analysis of stimulated electro photonic glow of liquids », *Water* (2010), 2 : 29-43.
[36] K. G. Korotkov, D. A. Korotkin, « Concentration dependence of gas discharge around drops of inorganic electrolytes *», J. Applied Phys.* (2001), 89(9) : 4732-4736.
[37] M. Skarja, M. Berden, I. Jerman, « Influence of ionic composition of water on the corona discharge around water drops », *J. Applied. Phys.* (1998), 84(5) : 2436-2442.
[38] Lou Jost, « Entropy and diversity », *Oikos* (2006), 113(2), 363-375.
[39] E. Marcon, « Mesure de la biodiversité et de la structuration spatiale de l'activité économique par l'entropie », *Revue Economique*, Presses de Sciences Po (2019), 70(3), pp.305. 10.3917/reco.703.0305. hal-02147526.
[40] T. O. Kvalseth, « Evenness indices once again : critical analysis of properties », *Kvalseth SpringerPlus* (2015) 4 : 232.
[41] A. González-Díez, J.A. Barreda-Argüeso, L. Rodríguez-Rodríguez, J. Fernández-Lozano. The use of filters based on the Fast Fourier Transform applied to DEMs for the objective mapping of karstic features. Geomorphology. Volume 385, 2021,
[42] Gerhard X. Ritter, Joseph N. Wilson, « Handbook of computer vision algorithms in image algebra », Second Edition (2001), CRC Press, Boca Raton.
[43] G. Ekman, "Weber's Law and Related Functions", *Journal of Psychology* (1959), 47 : 343-352
[44] Sergio Cesare Masin, Verena Zudini, Maura Antonelli, « Early alternative derivations of Fechner's law », *J. Hist. Behavorial Sci*. (2009), 45(1) : 56-65.
[45] Werner Frei, « Image enhancement by histogram hyperbolization », *Computer Graphics and Image Processing* (1977), 6 : 286-294.
[46] Daniel T. Cobra, José D. e Menezes Costa, F. Marcelo, « Realce de Imagens Através de Hiperbolizaçao do histograma », *Anais do SINGRAPI* (1992), pp. 63-71.
[47] Salem Saleh Al-amri, N. V. Kalyankar, S. D. Khamitkar, « Linear and non-linear contrast enhancement image », Int. J. Computer Sci. Network Security (2010), 10(2) : 139-143.
[48] Stephen M. Pizer, John D. Austin, John R. Perry, Hal D. safrit, « Adaptive histogram equalization for automatic contrast enhancement of medical images », Proc. SPIE 0626, Application of Optical Instrumentation in Medicine XIV and Picture Archiving and Communication Systems, (12 June 1986); https://doi.org/10.1117/12.975399.
[49] Adam Huang, Chung-Wei Lee, Hon-Man Liu, « Rolling ball sifting algorithm for the augmented visual inspection of carotid bruit auscultation », *Scientific Reports* (2016), 6 : 30179.
[50] C. A. Schneider, W. S. Rasband, K. W. Eliceiri, "NIH Image to ImageJ: 25 years of image analysis", *Nature methods* (2012), 9(7): 671-675.
[51] Chris Glasbey, Gerie van der Heijden, Vivian F. K. Toh, Alision Gray, « Colour display for categorical images », *Color research and application* (2007), 32(4) : 304-309.
[52] Mhemet Sezgin, Bülent Sankur, « Survey over image thresholding techniques and quantitative performance evaluation », J. Electronic Imaging (2004), 13(1) : 146-165.

[53] W. Doyle, "Operation useful for similarity-invariant pattern recognition", *Journal of the Association for Computing Machinery* (1962), 9 : 259-267.
[54] J. M. S. Prewitt, M. L. Mendelsohn, "The analysis of cell images," Annals New York Acad. Sci. (1966), 128 : 1035-1053.
[55] G. W. Zack, W. E. Rogers, S. A. Latt, S. A., « Automatic Measurement of Sister Chromatid Exchange Frequency », *Journal of Histochemistry and Cytochemistry* (1977), 25(7) : 741-753.
[56] T. W. Ridler, S. Calvard, « Picture thresholding using an iterative selection method », *IEEE Trans. on Systems, Man and Cybernetics* (1978), SMC-8 : 630-632.
[57] H. J. Trussel, « Comments on 'Picture thresholding using an iterative selection method' », *IEEE Trans. on Systems, Man and Cybernetics* (1979), SMC-9 : 311.
[58] A. Magid, R. Rotman, A. M. Weiss, , « Comment on 'Picture thresholding using an iterative selection method' », *IEEE Trans. on Systems, Man and Cybernetics* (1990), 20 : 1238-1239.
[59] Nobuyuki Otsu, « A threshold selection method from gray-level histogram », *IEEE Trans. on Systems, Man and Cybernetics* (1979), SMC-9 : 62-66.
[60] Wen-Hsiang Tsai, « Moment-preserving thresholding: a new approach », *Computer Vision, Graphics and Image Processing* (1985), 29 : 377-393.
[61] J. N. Kapur, P. K. Sahoo, A. K. C. Wong, "A New Method for Gray-Level Picture Thresholding Using the Entropy of the Histogram", *Graphical Models and Image Processing*. (1985), 29(3): 273-285.
[62] J. Kittler, J. Illingworth, "Minimum error thresholding," *Pattern Recognition* (1986) : 19 : 41-47.
[63] C. H. Li, C. K. Lee, « Minimum cross entropy thresholding », *Pattern Recognition* (1993), 26(4) :617-625.
[64] C. H. Li, P. K. S. Tam, « An iterative algorithm for minimum cross entropy thresholding », *Pattern Recognition Letters* (1998) 771-776.
[65] C. A. Glasbey, "An analysis of histogram-based thresholding algorithms", *CVGIP: Graphical Models and Image Processing* (1993), 55(6) : 532-537.
[66] A. G. Shanbhag, "Utilization of Information Measure as a Means of Image Thresholding", *Graphical Models and Image Processing* (1994), 56(5): 414-419.
[67] J. C. Yen, F. J. Chang F.J., S. Chang, "A New Criterion for Automatic Multilevel Thresholding", *IEEE Trans. on Image Processing* (1995), 4(3): 370-378.
[68] L.-K. Huang, M.-J. J. Wang, "Image Thresholding by Minimizing the Measures of Fuzziness", *Pattern Recognition* (1995), 28(1): 41-51.
[69] P. Sahoo, C. Wilkins, J. Yeager, ''Threshold selection using Renyi's entropy,'', *Pattern Recognition* (1997), 30 : 71-84.
[70] J. Bernsen, "Dynamic Thresholding of Grey-Level Images", *Proc. of the 8th Int. Conf. on Pattern Recognition* (1986), pp. 1251-1255.
[71] Can Eyupoglu, « Implementation of Bernsen's locally adaptive binarization method for gray scale images », The Online Journal of Science and Technology (2017), 7(2) : 68-72.
[72] W. Niblack, "An introduction to Digital Image Processing", Prentice-Hall (1986), Englewood Cliffs, New Jersey, pp. 115-116.
[73] J. Sauvola and M. Pietaksinen, "Adaptive document image binarization", *Pattern Recognition* (2000), 33 : 225–236.
[74] Neerad Phansalkar, Sumit More, Ashish Sabale, Madhuri Joshi, "Adaptive local thresholding for detection of nuclei in diversity-stained cytology images", *International Conference on Communications and Signal Processing* (2011), 218-220.

[75] Andreas E. Savakis, "Adaptive document image thresholding using foreground and background clustering", *Proceedings of International Conference on Image Processing*, Intl. Conf. Image Process. ICIP'98, Chicago, October (1998).
[76] Duong Anh Duc, Tran Le Hong, Tran Duc Duan, "Optimizing speed for adaptative local thresholding algorithm using dynamic programming, "The 7th International Conference on Electronics, Information and Communications (ICEIC'04), (2004), 1 : 438-441.
[77] Stephen B. Gray, « Local properties of binary images in two dimensions », *IEEE Transactions on Computers* (1971), C20 : 551-561.
[78] Luren Yang, Fritz Albregtsen, Tor Lonnestad, Per Grottum, « Methods to estimate areas and perimeters of blob-like objects : a comparison », *IAPR Workshop on Machine Vision Applications* (1994), Dec. 13-15, pp. 272-276.
[79] P. L. Rosin, "Measuring Shape: Ellipticity, Rectangularity, and Triangularity", *Machine Vision and Applications* (2003) 14: 172-184.
[80] R. Haralick and L. Shapiro, Computer and Robot Vision. Reading, Mass.: Addison-Wesley, 1992.
[81] Ming_kuei Hu, « Visual pattern recognition by moments invariants », *IRE Transactions on Information Theory* (1962), Februrary, pp. 179-187.
[82] Jan Flusser, Tomas Suk, « Pattern recognition by affine moment invariants », *Pattern Recognition* (1993), 26(1) : 167-174.
[83] Jan Flusser, « On the independence of rotation moments invariants», *Pattern Recognition* (2000), 33: 1405-1410.
[84] Jan Flusser, Tomas Suk, « Rotation moments invariants for recognition of symmetric objects », *IEEE Transactions on Image Processing* (2006), 15(12) : 3784-3790.
[85] H. Freeman, "On the Encoding of Arbitrary Geometric Configurations", *IRE Transactions on Electronic Computers* (1961), 10: 260-268.
[86] A. M. Andrew, "Another Efficient Algorithm for Convex Hulls in Two Dimensions", *Info. Proc. Letters* (1979), 9: 216-219.
[87] G. T. Toussaint, "Solving Geometric Problems with the Rotating Calipers" *Proc. of the IEEE MELECON'83 Conf.* (1983), Athens, Greece, May, pp. 1-8.
[88] J. Kilday F. Palmieri F., M. D. Fox, "Classifying Mammographic Lesions Using Computerized Image Analysis" *IEEE Trans. on Medical Imaging* (1993), 12(4): 664-669.
[89] L. M. Bruce, M. Kallergi, "Effects of Image Resolution and Segmentation Method on Automated Mammographic Mass Shape Classification", *Proc. of the SPIE* (1999), 3661: 940-947.
[90] L. Gupta, M. D. Srinath, « Contour sequence moments for the classification of closed planar shapes », *Pattern Recognition* (1987), 20(3) : 267-272.
[91] Andrew Fitzgibbon, Maurizio Pilu, Robert B. Fisher, « Direct least square fitting of ellipses », *IEEE transactions on Pattern Analysis and Machine Intelligence* (1999), 21(5) : 476-480.
[92] B. Peirce, « Criterion for the rejection of doubtful observations », *The Astronomical Journal* (1852), 45 : 161-163.
[93] B. A. Gould Jr., « On Peirce's criterion for the rejection of doubtful observations, with tables for facilitating its application », *The Astronomical Journal* (1855), 83 : 81-87.
[94] K. A. Sankpal, « A Review on Data Normalization Techniques ». *International Journal of Engineering Research & Technology* (June-2020),Vol. 9 Issue 06 : 1438-1441.